



The self-assembly and metal adatom coordination of a linear bis-tetrazole ligand on Ag(111)[†]

Cite this: *Chem. Commun.*, 2018, 54, 10072

Received 30th May 2018,
Accepted 14th August 2018

DOI: 10.1039/c8cc04323j

rsc.li/chemcomm

Peter Knecht,^a Nithin Suryadevara,^b Bodong Zhang,^a Joachim Reichert,^a Mario Ruben,^{id bc} Johannes V. Barth,^{id a} Svetlana Klyatskaya^{*b} and Anthoula C. Papageorgiou^{id *a}

We employ a linear linker molecule consisting of a benzene functionalised with two tetrazole moieties at *para* positions. Its self-assembly and coordination with the native silver adatoms and codeposited Fe adatoms on a Ag(111) surface under ultra high vacuum conditions are investigated by means of scanning tunnelling microscopy and X-ray photoelectron spectroscopy. We discover a rich spectrum of room-temperature stable Ag and Fe²⁺ coordination nodes depending on the formation temperature.

The functionalisation of metal surfaces with azole compounds and in particular triazole and tetrazole compounds has attracted interest due to their corrosion inhibiting properties.¹ More recently, triazole and tetrazole ligands have been employed in the formation of coordination polymers with functional properties ranging from fluorescence² and second harmonic generation² to spin crossover (SCO) phenomena.³ The tetrazole group with its four nitrogen atoms is known to show distinct types of coordination nodes for the formation of metal organic coordination networks. While the tetrazole can act as both a dinucleating ligand and a trinucleating ligand, the deprotonated tetrazolate can engage in coordination bonds with up to four metal atoms.⁴ Here we investigate 1,4-di(1*H*-tetrazole-5-yl)benzene (BTB), consisting of a benzene with tetrazole groups at the 1 and 4 positions (Fig. 1), as a promising ligand for metal-organic frameworks: it couples the coordination properties of two tetrazole ligands and offers tunability of size *via* implementation of additional backbone units. Metal-organic frameworks with Ag,⁵ Cu,⁵ and Fe³ nodes

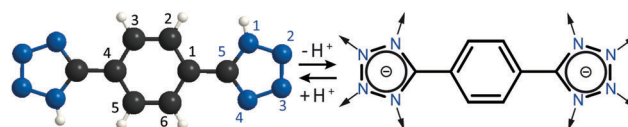


Fig. 1 Ball-and-stick model of 1,4-bis(1*H*-tetrazole-5-yl)benzene (BTB) and possible coordination modes of the tetrazolate anion. Carbon, nitrogen and hydrogen atoms are black, blue and white, respectively. The atom numbering is indicated.

are reported to form under hydrothermal conditions and have demonstrated SCO phenomena.³

To the best of our knowledge the surface coordination chemistry of tetrazoles is hitherto unexplored, although compounds with the related triazole group have been studied. On the more inert Au(111) hydrogen bonding drove the self-assembly of benzotriazole.⁶ On Cu(111) triazoles are found to bind with a triazole group either oriented towards the substrate or creating a planar node with a native Cu adatom.⁷ On HOPG the addition of Cu adatoms results in the formation of Cu²⁺.⁸

Here we investigate the afore described tetrazole linear linker (Fig. 1) under ultra-high vacuum conditions *via* scanning tunnelling microscopy (STM) to obtain real space images of the self-assembly with molecular resolution, and X-ray photoelectron spectroscopy (XPS) to get information about the chemical state of the elements on the surface. We thus gain the first experimental atomistic scale insight of the binding of tetrazole moieties on Ag(111). Furthermore, we exploit our *in situ* sample preparation methodology for the formation of such metal-organic networks at the vacuum-solid interface, which combines a clean synthesis without any solvents with a great control of the thickness by adjusting the dose of sublimed molecules.⁹ We note that two dimensional (2D) metal organic coordination networks are a current topic of intense investigation,¹⁰ and recently enhanced cooperativity for supported SCO networks was predicted.¹¹

Initially, we investigate the room temperature (RT, ~300 K) self-assembly of BTB on the Ag(111) surface, where mobile Ag adatoms are known to be present.¹² Shortly after the molecular

^a Physics Department E20, Technical University of Munich, D-85748 Garching, Germany. E-mail: a.c.papageorgiou@tum.de

^b Institute of Nanotechnology, Karlsruhe Institute of Technology, D-76344 Eggenstein-Leopoldshafen, Germany. E-mail: svetlana.klyatskaya@kit.edu

^c Institute de Physique et Chimie de Matériaux (IPCMS), CNRS-Université Strasbourg, 23 rue du Loess, BP 43, F-67034 Strasbourg Cedex 2, France

[†] Electronic supplementary information (ESI) available: Experimental procedures; BTB crystal structure; additional STM images, models and XPS data; quantitative XPS analysis, illustrations of chiral recognition and switches; overview of polymorphism. See DOI: 10.1039/c8cc04323j

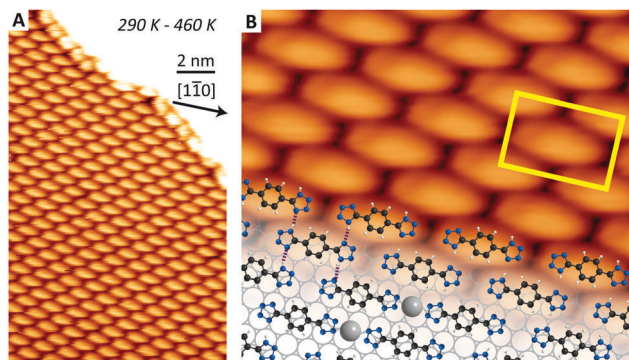


Fig. 2 RT self-assembly of BTB on Ag(111) (phase α , observed after annealing in the indicated temperature range). (A) Large scale STM image (-1.25 V, 90 pA), the Ag $[1\bar{1}0]$ direction is indicated. (B) Detailed STM image (1.25 V, 110 pA) overlaid with a model. The unit cell is marked in yellow. The ball-and-stick model is based on the crystal structure.¹³ Black, blue, and white spheres represent carbon, nitrogen and hydrogen, respectively. Grey spheres mark possible position of metal adatoms (Ag and/or Fe). Empty grey circles represent substrate atoms. Purple dotted lines indicate hydrogen bonding between nitrogen atoms.

deposition, elongated protrusions appear on the STM images along the $[1\bar{1}0]$ direction (Fig. 2), coexisting with a 'sea' of diffusing molecules. These protrusions are consistent with the molecular dimensions of BTB adsorbing planarly on the metallic surface. The overview image in Fig. 2A evidences the formation of a self-assembled close-packed two-dimensional island (phase α), which is characterized by a commensurate unit cell $(5, 0|2, 4)$ (see Fig. 2B) and has been the sole structure observed after annealing to temperatures of up to 390 K.

We propose that these islands consist of BTB in the *trans* configuration (Fig. 2B). Here each unit cell contains two BTB *trans* molecules, one in each surface enantiomeric form; that is the two molecular *trans* configurations in this model result by a mirror and translation operation and cannot arise from any combination of rotation plus translation operations. The structure is stabilised by the $\text{NH}\cdots\text{N}$ hydrogen bondings indicated by purple dotted lines in Fig. 2B. The proposed model is in analogy to the hydrogen bonded structures found in single crystals of BTB (Fig. S1, ESI †),¹³ with the projected $\text{N}\cdots\text{N}$ separation measured as 2.9 Å vs. 2.8 Å.¹³ We note that in the STM the two isomeric forms cannot be distinguished and it is also possible to model phase α solely with *cis* isomers (Fig. S2, ESI †). The spacing of the tetrazole units along the Ag $[1\bar{1}0]$ and the epitaxial unit cell is consistent with a scenario whereupon Ag adatoms are located at bridge sites and further stabilise the network by metal coordination (Fig. 2B). The Ag adatom was not directly evidenced in our STM data, similarly to Ag adatoms in coordination nodes of two *ortho*-benzoquinone moieties.¹⁴ This type of on-surface coordination is not unprecedented on Ag(111) (coordination of four iminic N atoms with a Ag adatom after annealing at 383 – 443 K was proposed recently,¹⁵ whereas free base porphyrins are complexing Ag after annealing above 530 K).¹⁶ However, this would be the first report of such coordination on surfaces already at room temperature and its plausibility will be discussed along with the XPS data.

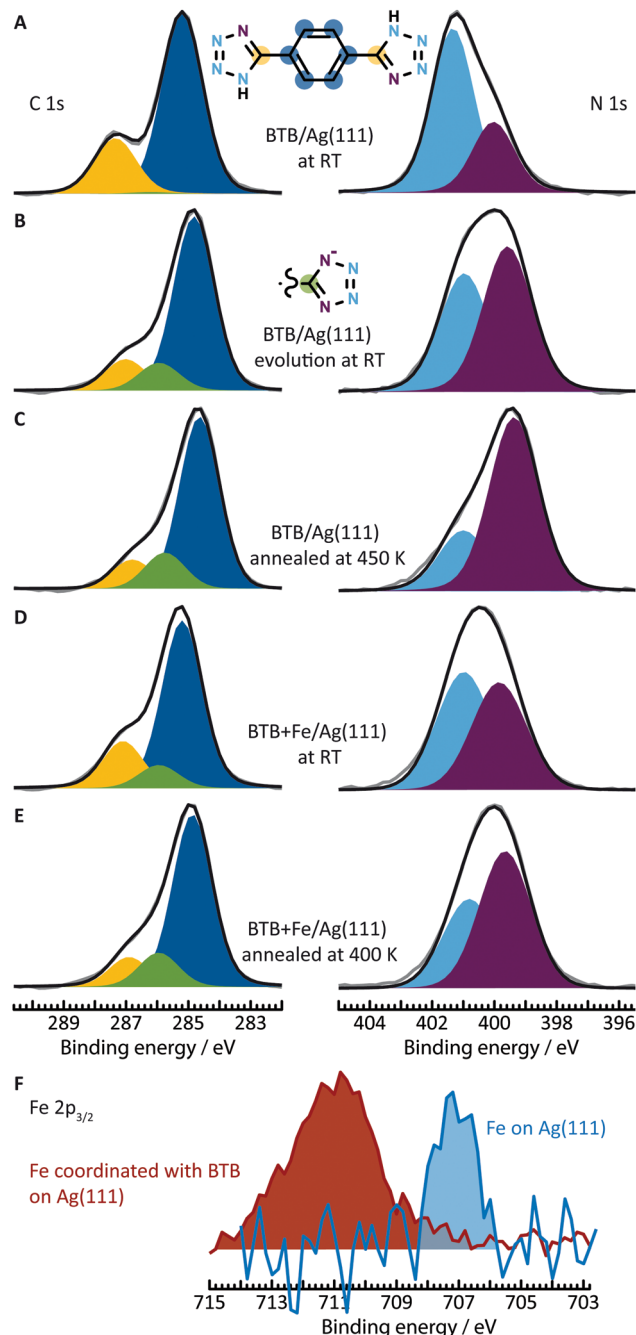


Fig. 3 XPS measurements. (A–E) C 1s and N 1s regions corresponding to: (A) ~ 1 monolayer of BTB on Ag(111) at RT showing intact molecules after sublimation; (B) deprotonation of aminic N atoms and Ag coordination occurring slowly at RT (recorded 18 h after sublimation); (C) higher degree of N deprotonation and Ag adatom coordination after annealing at 450 K (~ 4 h after sublimation). (D) Monolayer BTB and Fe atoms in a ratio of $\sim 6:1$ (Tables S1 and S2, ESI †) dosed sequentially on Ag(111) at RT evidencing both deprotonation of aminic N and coordination of iminic N to Fe (~ 2 h after sublimation); (E) both of these processes are promoted by annealing to 400 K (~ 4 h after sublimation). (F) Fe $2p_{3/2}$ spectra for Fe on the bare Ag(111) surface (blue, 707.2 eV) and Fe with excess BTB on Ag(111) (red, 711.0 eV) show that all the Fe is coordinated with the tetrazole moieties and shifts to a higher oxidation state.

Complementary XPS measurements confirmed that the intact molecule was present on the Ag(111) following RT deposition.

The relevant C 1s spectrum (Fig. 3A, left) shows two main components, which can be related to the carbon atoms of the benzene (285.2 eV, blue) and the tetrazoles (287.3 eV, yellow), respectively, with the expected ratio of $\sim 3:1$. In the corresponding N 1s spectrum, we also identify two peaks at 401.3 eV (blue) and 400.0 eV (violet) in a ratio of $\sim 3:1$. The former corresponds to the combined contribution of the aminic N^{17,18} and iminic N atoms bound to two nitrogen atoms,¹⁹ the latter to the iminic N atoms bonded to a single N atom.^{19,20}

XPS reveals that at RT the deprotonation of the N1 atoms occurs slowly and concomitantly with N–Ag coordination at the N2/N3 atoms. Fig. 3B shows measured spectra on the same samples as the one shown in Fig. 3A, albeit recorded ~ 18 h later (see Fig. S3 for spectra at intermediate time intervals, ESI[†]). The lower energy component of the N 1s region (Fig. 3B right) increases in relative intensity, as a result of a shift of the N1 contribution by ~ 1.3 eV towards lower binding energy, commonly associated with aminic N deprotonation.¹⁷ The C 1s spectrum (Fig. 3B, left) shows a splitting of the peak related to the tetrazole carbon.²¹ However, one can notice that the C 1s signal reveals only $\sim 50\%$ of the tetrazole units to be deprotonated as the intensities of the components at 287.0 eV (yellow in Fig. 3B) and 286.0 eV (green in Fig. 3B corresponding to deprotonated nearest N neighbour) are approximately equal. Therefore the total intensity of the N 1s component at 399.6 eV has further contribution from a shift of the iminic N components with two N nearest neighbours (for relative intensities of different components see Table S1, ESI[†]). Such a shift would be consistent with a scenario of metal coordination with Ag adatoms.²¹ These observations substantiate the model with Ag adatoms in the densely packed phase α (Fig. 2B).

Upon annealing the sample at 430 K, two additional phases β and γ can be observed by STM measurements (see Fig. 4). The amount of deprotonated tetrazoles is $\sim 60\%$ after annealing (ratio of green component to total contributions from tetrazole carbon atoms in Fig. 3C, left). We therefore infer that the N1 of both tetrazole moieties of each molecule are deprotonated in phases β and γ .

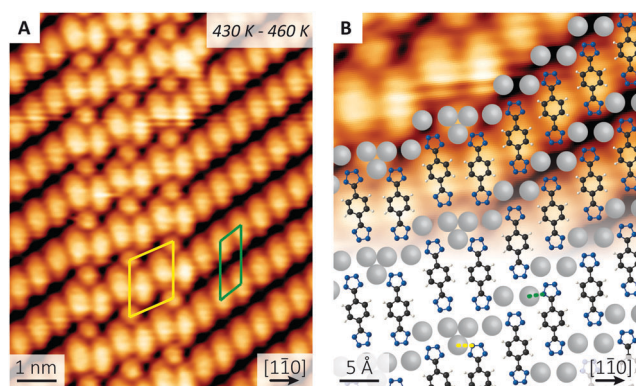


Fig. 4 Ag adatom coordination of BTB. (A) STM image (1.75 V, 110 pA) of the structures formed after annealing in the indicated temperature range, unit cells of phases β and γ in green and yellow, respectively. (B) Molecular model including Ag adatoms (grey spheres). The shortest Ag–N bonds are depicted in green and yellow for phases β and γ , respectively.

In phase β (green unit cell in Fig. 4A) the presence of Ag adatoms is inferred based on the XPS evidence of Fig. 3C, which shows the majority of N signal shifted to lower binding energy as a combined effect of N deprotonation and N–Ag coordination. STM images seldom evidenced the presence of single Ag adatoms (Fig. S4, ESI[†]). We propose two Ag adatoms between the tetrazole groups of two molecules with a projected Ag–N distance of ~ 2.2 Å (indicated in Fig. 4B), which is in good accordance with reported Ag–N bond lengths of tetrazole moieties.²² The molecules assemble in a higher order coincidence superlattice (three different adsorption sites on the Ag(111) substrate) with the epitaxy matrix (8/3, 5/3|3, 6). In phase γ (yellow unit cell in Fig. 4A), the presence of Ag adatoms can be identified in the STM image as broad round protrusions. Close inspection of the unit cell dimensions reveals that each of these protrusions is best fitted with three Ag adatoms. Similar nanodots have been observed with Cu adatoms in two dimensional coordination networks.²³ Two additional Ag adatoms per unit cell are evidenced under the same imaging conditions as the adatoms in phase β (Fig. S4, ESI[†]). We therefore infer that single Ag adatoms are not necessarily visible in STM images, whereas a trimer of Ag adatoms would be routinely discernible. The projected Ag–N distances between nitrogen atoms of the tetrazoles and silver adatoms are 2.3 Å. The unit cell comprises two molecules and five Ag adatoms and is commensurate: (5, 2|3, 6). Transitions between both structures, β and γ , can be observed along the Ag[1 $\bar{2}$ 1] directions and exhibit organisational chiral recognition (Fig. S5, ESI[†]).

Targeting metal–organic networks with magnetic properties, such as SCO phenomena, we explored the coordination with Fe. This occurs readily at RT after sublimation of BTB and Fe adatoms on the clean Ag(111) surface, identified by an Fe oxidation state, distinctively different than metallic Fe on Ag(111) (Fig. 3F) and consistent with literature values of Fe²⁺/Fe³⁺.²⁴ As under these conditions, the STM images do not identify any other structure formation as the densely packed phase α , the Fe is assumed to be incorporated in that phase similarly as proposed in the model in Fig. 2B (grey spheres). Since the molecular XPS signatures do not change significantly in the presence of Fe adatoms, we propose that Fe displaces Ag in the coordination nodes. Based on the number of tetrazole ligands and the Fe 2p binding energy we ascribe the Fe oxidation state in these nodes to 2+. The projected Fe–N distances in these structures (2.3 Å) are close to Fe–N bond lengths (2.2 Å) in high spin Fe²⁺.³

Two distinct phases (δ and ϵ , Fig. 5) associated with the presence of Fe on the surface can be found in STM investigations of Ag(111) surfaces prepared by sequential dosing of BTB and Fe and subsequent annealing to 390 K and 430 K, respectively. In phase δ (Fig. 5A and B) one can identify pairs of small round protrusions in between molecular ligands, which can be tentatively assigned to dimers of Fe atoms (separated by 3.3 Å, see also Fig. S7A, ESI[†]). The head-to-head Fe coordination of the tetrazole moieties is reminiscent of the *exo* ligation reported for surface stabilized dehydrogenated pyrazole moieties.²⁵ Phase δ is characterised by a unit cell of five BTB molecules and four Fe atoms: (6, 1|4, 10). The molecular domains have a zig-zag appearance which arise from chirality and orientational switches of the rows along the

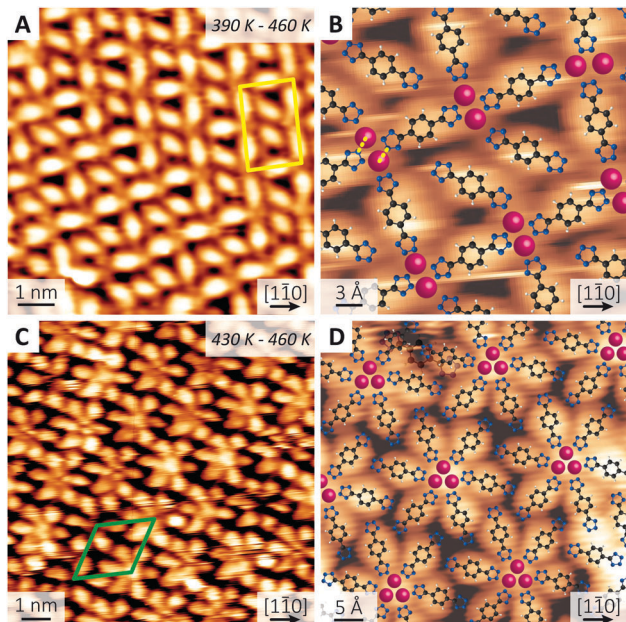


Fig. 5 Fe coordination of BTB after annealing in the indicated temperature range. (A) STM of phase δ (1.50 V, 60 pA) with rows of alternating chirality. The unit cell is marked in yellow. (B) Detail of phase δ (1.50 V, 60 pA). The shortest Fe–N distances are marked in yellow. Magenta spheres represent Fe adatoms. (C) STM of phase ϵ (1.50 V, 110 pA), the unit cell is marked in green. (D) Detail of phase ϵ (1.50 V, 110 pA).

$[1\bar{2}1]$ directions of the Ag(111) (Fig. S6, ESI[†]). Phase ϵ has a structure resembling flowers (Fig. 5C and D). Each unit cell consists of six molecules and presumably three Fe atoms imaged as three round protrusions (see also Fig. S7B, ESI[†]): (8, 1|7, 8).

In summary, we have systematically characterised at the atomic scale the self-assembly of a linear bis-tetrazole linker molecule on Ag(111). Unexpectedly, simultaneous deprotonation and coordination with native Ag adatoms of the tetrazole moieties occur slowly at RT and are further enhanced by annealing to higher temperatures. Owing to the multitude of coordination sites offered by the tetrazole moiety, polymorphism is found in the metal adatom coordination motifs (for an overview see Fig. S8, ESI[†]). These range from hosting Ag/Fe trimers to dimers and single adatoms. We thus provide an atomistic scale model of how the silver surface is modified by the adsorption of a planar tetrazole compound and the involvement of metal adatoms in its binding, which is expected to contribute to the mechanistic understanding of corrosion inhibition. Intriguingly, BTB–Fe coordination on the Ag/vacuum interface results in Fe²⁺ species, implying that this ligation might prevent the interfacial charge

transfer which often lowers the observed oxidation state and quenches the native magnetic properties of metal–organic complexes.²⁶ Further experiments are necessary to determine its spin state and whether it exhibits SCO phenomena. At last, we identified a structure (densely packed, phase α) of BTB on Ag(111) which can accommodate metal adatoms coordinating the tetrazoles without changing noticeably the positions of the molecular ligands, presumably mediated by the tetrazole deprotonation.

Financial support was provided by of German Research Foundation (DFG) through the priority programme 1928 COOR-NETs. B. Z. was funded by the China Scholarship Council (CSC). The authors acknowledge the KNMF facility (KIT, Germany).

Conflicts of interest

There are no conflicts to declare.

References

- (a) M. M. Antonijevic and M. B. Petrovic, *Int. J. Electrochem. Sci.*, 2007, **2008**, 1–28; (b) Y. I. Kuznetsov and L. P. Kazansky, *Russ. Chem. Rev.*, 2008, **77**, 219–232.
- H. Zhao, *et al.*, *Chem. Soc. Rev.*, 2008, **37**, 84–100.
- Z. Yan, *et al.*, *Chem. Commun.*, 2012, **48**, 3960–3962.
- G. Aromí, *et al.*, *Coord. Chem. Rev.*, 2011, **255**, 485–546.
- A. Maspero, *et al.*, *Inorg. Chim. Acta*, 2009, **362**, 4340–4346.
- F. Grillo, *et al.*, *Nanoscale*, 2016, **8**, 9167–9177.
- (a) F. Grillo, *et al.*, *J. Phys. Chem. C*, 2014, **118**, 8667–8675; (b) F. Grillo, *et al.*, *Nanoscale*, 2013, **5**, 5269–5273; (c) S. J. Jethwa, *et al.*, *ACS Nano*, 2017, **11**, 8302–8310.
- L. Cui, *et al.*, *Sci. Rep.*, 2016, **6**, 25544.
- I. Stassen, *et al.*, *Chem. – Eur. J.*, 2016, **22**, 14452–14460.
- (a) L. Dong, *et al.*, *Prog. Surf. Sci.*, 2016, **91**, 101–135; (b) N. Lin, *et al.*, *Top. Curr. Chem.*, 2009, **287**, 1–44; (c) J. V. Barth, *Surf. Sci.*, 2009, **603**, 1533–1541; (d) R. Gutzler, *et al.*, *Acc. Chem. Res.*, 2015, **48**, 2132–2139; (e) D. Ćeija, *et al.*, *Acc. Chem. Res.*, 2018, **51**, 365–375.
- T. Groizard, *et al.*, *J. Phys. Chem. Lett.*, 2017, **8**, 3415–3420.
- (a) K. Morgenstern, *et al.*, *Phys. Rev. Lett.*, 1996, **76**, 2113–2116; (b) M. Poensgen, *et al.*, *Surf. Sci.*, 1992, **274**, 430–440.
- J.-H. Deng, *et al.*, *Inorg. Chem. Commun.*, 2010, **13**, 1585–1589.
- A. C. Papageorgiou, *et al.*, *Nanoscale*, 2018, 9561–9568.
- C. G. Williams, *et al.*, *J. Phys. Chem. C*, 2017, **121**, 13183–13190.
- A. Wiengarten, *et al.*, *J. Am. Chem. Soc.*, 2014, **136**, 9346–9354.
- J. S. Stevens, *et al.*, *Cryst. Growth Des.*, 2015, **15**, 1776–1783.
- A. C. Papageorgiou, *et al.*, *ACS Nano*, 2012, **6**, 2477–2486.
- E. Szócs, *et al.*, *Electrochim. Acta*, 2004, **49**, 1371–1378.
- A. Katrib, *et al.*, *J. Electron Spectrosc. Relat. Phenom.*, 1983, **31**, 317–321.
- G. Xue, *et al.*, *J. Am. Chem. Soc.*, 1988, 2393–2395.
- T. Wu, *et al.*, *Inorg. Chem. Commun.*, 2006, **9**, 341–345.
- F. Bebensee, *et al.*, *Angew. Chem., Int. Ed.*, 2014, **53**, 12955–12959.
- A. P. Grosvenor, *et al.*, *Surf. Interface Anal.*, 2004, **36**, 1564–1574.
- A. Shchyrba, *et al.*, *J. Am. Chem. Soc.*, 2014, **136**, 9355–9363.
- S. Vijayaraghavan, *et al.*, *ACS Nano*, 2015, **9**, 3605–3616.